Lecture 9-1 Thermal Actuators

◆ Thermal Actuator fundamental

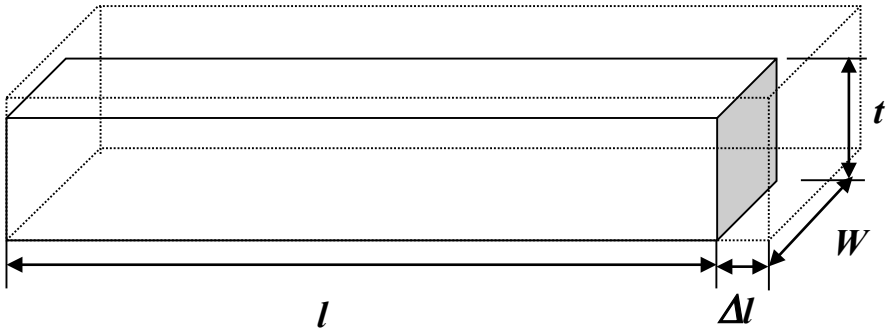

CTE: Coefficient of Thermal Expansion (linear range)

$$CTE: \quad \alpha \equiv \frac{\Delta l}{l}\frac{1}{\Delta T} \tag{9-1}$$

where: l is the length, ΔT is the temperature difference

Notice:

a. **CTE is approximately constant for a considerable rage of temperature (in general, the coefficient increases with an increase of temperature)**
b. **For homogeneous and isotropic material, the coefficient applied to all dimensions (directions).**
c. **CTE of some materials:**

Table 3-14 Coefficient (α) of linear thermal expansion of some materials (per °Cx10^{-6})

Material	α	Material	α
Alnico I (Permanent magnet)	12.6	Nylon	90
Alumina (polycrystalline)	8.0	Phosphor-bronze	9.3
Aluminum	25.0	Platinum	9.0
Brass	20.0	Plexiglas (Lucite)	72
Cadmium	30.0	Polycarbonate (ABS)	70
Chromium	6.0	Polyethylene (high density)	216
Comol (Permanent magnet)	9.3	Silicon	2.6
Copper	16.6	Silver	19.0
Fused quartz	0.27	Solder 50-50	23.6
Glass (Pyrex®)	3.2	Steel (SAE 1020)	12.0
Glass (regular)	9.0	Steel (stainless: type 304)	17.2
Gold	14.2	Teflon	99
Indium	18.0	Tin	13.0
Invar	0.7	Titanium	6.5
Iron	12.0	Tungsten	4.5
Lead	29.0	Zinc	35.0
Nickel	11.8		

From Eq. (9-1), for the thermal induced strain:

$$\varepsilon_{therm} \equiv \frac{\Delta l}{l} = \alpha \Delta T \qquad \textbf{(9-2)}$$

For a beam clamped between two walls, the induced stress and total force are:

$$F_{therm} = A\sigma = AE\varepsilon_{therm} = WtE\alpha\Delta T \qquad \textbf{(9-3)}$$

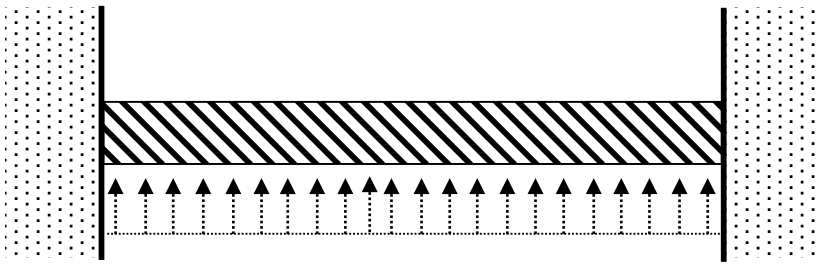

Heat

For a silicon beam, α=2.6×10^{-6} m/m°C, *l*=100 μm, W=t=10 μm,

and ΔT=100 °C, E~10^{11} Pa, $C_{p,si}$=0.714 KJ/Kg°C

$$F=WtE\alpha\Delta T=2.6\ mN$$

$$\Delta l=l\alpha\Delta T=26\ nm$$

⇨ **large force, small displacement!!**

Input energy:

$$W_{in}=C_{p,si}m\Delta T=714\ pJ$$

Output energy:

$$W_{out}=\int_0^{\Delta L}Fdx=\int_0^{\Delta L}\frac{AEx}{L}dx=\frac{AE}{2L}(\Delta L)^2=26.45\quad pJ$$

Efficiency: 3.7 % => Low efficiency!!

How to magnify the displacement?

1. Extending arm

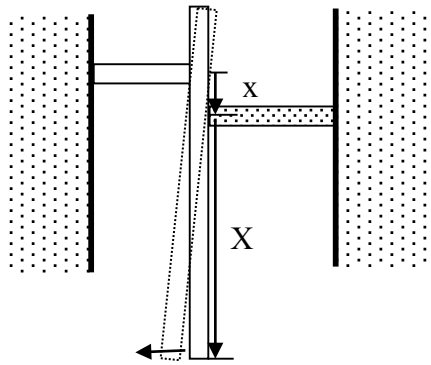

Displacement increases by X/x, but force decreases by x/X (for rigid vertical beam, and heating only the right side horizontal bar)

2. Different beam width

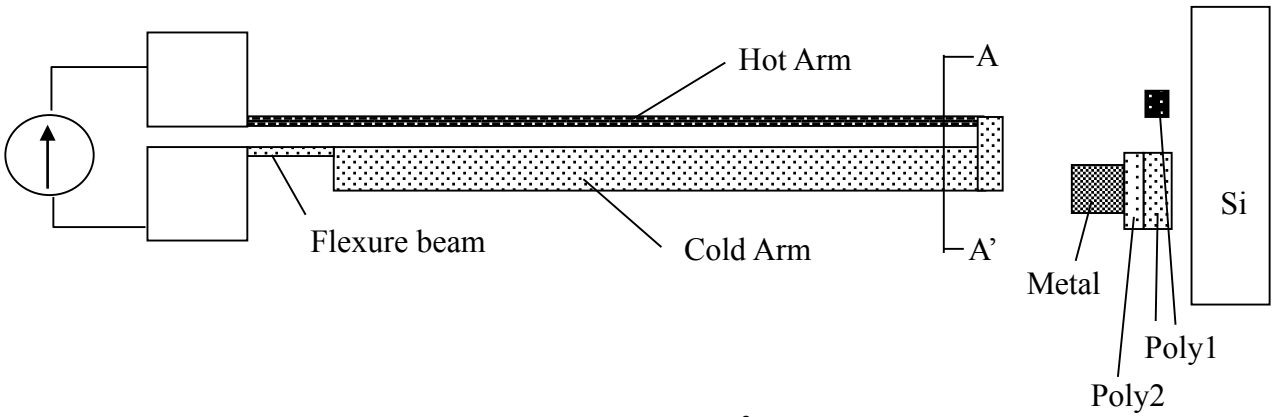

Power Dissipation=I^2R => $P \propto R$,

here $R = \frac{\rho A}{L}$ **and I=constant**

=> Hot arm has much larger resistance

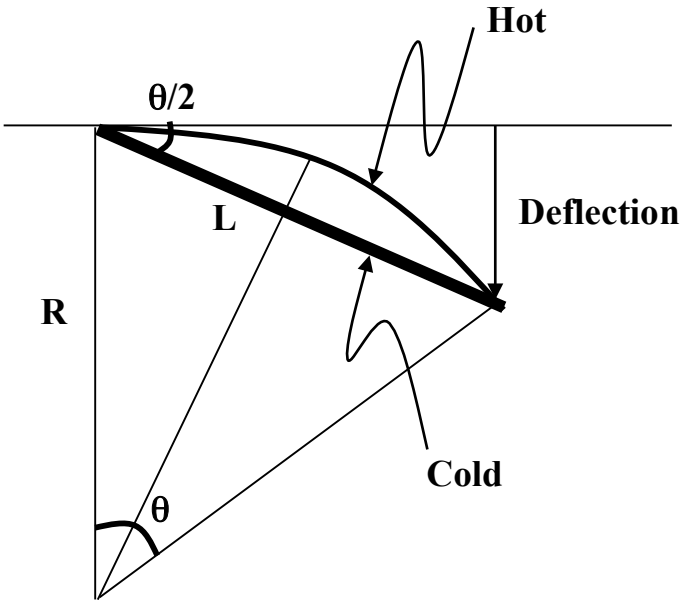

Arc length = $R\theta$ = Hot Arm length

Chord length L= (R sin(θ/2))×2= cold arm length

$$\Delta L = R\theta - 2R\sin\frac{\theta}{2}$$

$$\frac{\Delta L}{L} = \frac{\theta - 2\sin\frac{\theta}{2}}{2\sin\frac{\theta}{2}} = \alpha\Delta T$$

Use Taylor expansion => $\theta = \sqrt{24\alpha\Delta T}$

$$D = L \times \sin\frac{\theta}{2} = (2R\cdot\sin\frac{\theta}{2})\sin\frac{\theta}{2}$$

$$\frac{D}{\Delta L} = \frac{(2R\cdot\sin\frac{\theta}{2})\sin\frac{\theta}{2}}{R(\theta - 2(\frac{\theta}{2} - \frac{\theta^3}{48}))} \approx \frac{12}{\theta} \approx 160 \quad for\ \Delta T = 100°C$$

=> Magnify displacement to 160 times !!

3. Bimorph beam

(ii) Composite plate

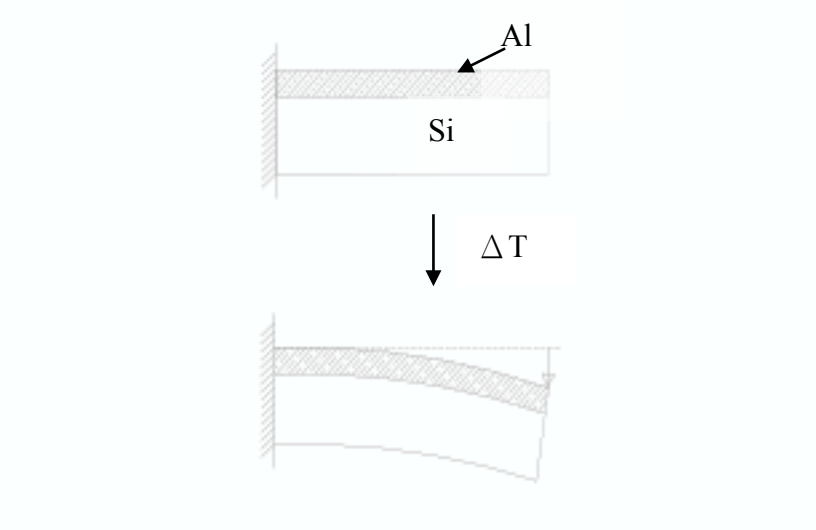

Al: E_{Al}=73Gpa; β_{Al}=22.5e-6 m/m/℃

Si: Esi=10e11Pa; β_{Si}=2.3e-6 m/m/℃

Analysis:
Assume
1.Al much thinner than Si
2.Biaxial Stress
3.Plane Remain plane (No warp)
3D isotropic system:

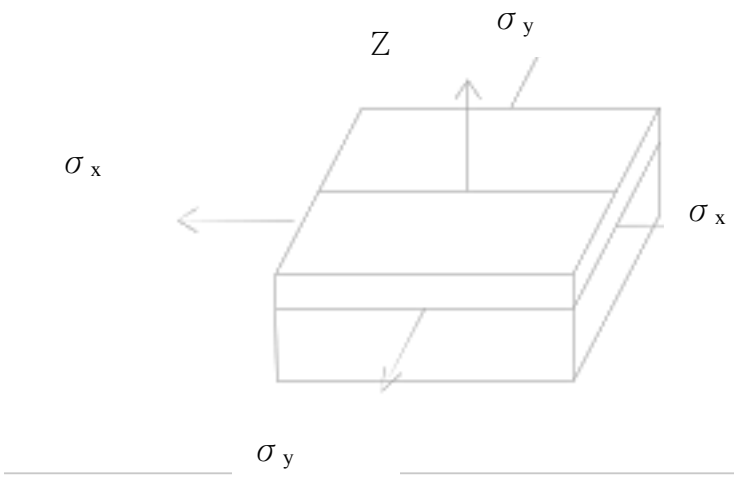

$$\varepsilon_x = \frac{1}{E}\left[\sigma_x - \nu\left(\sigma_y + \sigma_z\right)\right]$$

$$\varepsilon_y = \frac{1}{E}\left[\sigma_y - \nu\left(\sigma_z + \sigma_x\right)\right]$$

$$\varepsilon_z = \frac{1}{E}\left[\sigma_z - \nu\left(\sigma_x + \sigma_y\right)\right]$$

where ν **:Poisson's ratio**

Biaxial stress => $\sigma_z = 0$, $\sigma_x = \sigma_y$

$$\Rightarrow \varepsilon_x = \varepsilon_y = \frac{1-\nu}{E}\sigma_{x(\mathrm{ORG})} \text{ , } \varepsilon_z = -\frac{2\nu\sigma}{E}$$

$$\Rightarrow \sigma_x = \frac{E}{1-\nu}\varepsilon_x \rightarrow \textbf{Replace } E \textbf{ with } \frac{E}{1-\nu}$$

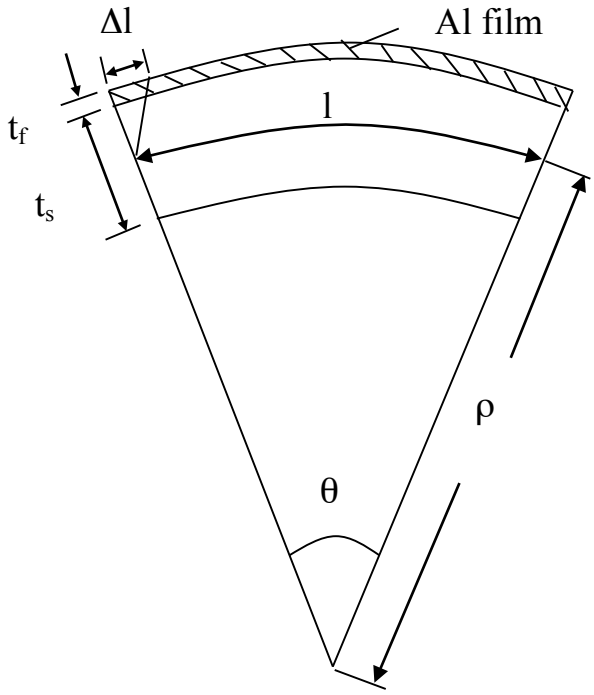

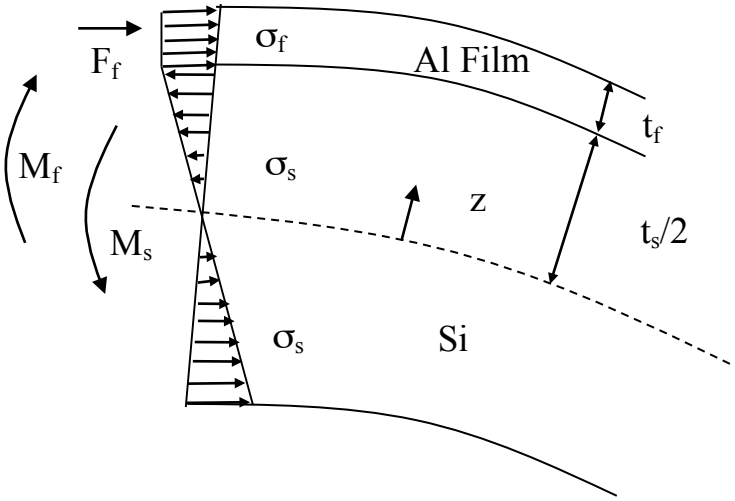

what's is ρ ? and M_f ?

(1) Geometry

Si deformation at Boundary= Al film deformation

$$\ell + \ell\beta_s\Delta T + \Delta\ell = \ell + \ell\beta_f\Delta T - \ell\varepsilon_f$$

Here: $\dfrac{\Delta\ell}{\frac{t_s}{2}} = \dfrac{\ell}{\rho}$ => $\Delta\ell = \dfrac{\ell}{\rho}\dfrac{t_s}{2}$

$$\varepsilon_f = \left(\frac{1-\nu}{E}\right)_f \sigma_f$$

$$\frac{t_s}{2\rho} + \left(\frac{1-\nu}{E}\right)_f \sigma_f = \left(\beta_f - \beta_s\right)\Delta T \qquad \textbf{(1)}$$

(2) Moment balance

$$M_f = \sigma_f \cdot W \cdot t_f \cdot \frac{t_s}{2} \tag{2}$$

$$M_s = w\int_{-t_s/2}^{t_s/2} z\sigma(z)dz = w\int_{-t_s/2}^{t_s/2} \left(\frac{E}{1-\nu}\right)\frac{z^2}{\rho}dz \tag{3}$$

$$= \left(\frac{E}{1-\nu}\right)_s \frac{wt_s^{\,3}}{12\rho}$$

$$M_f = M_s$$

$$\sigma_f = \left(\frac{E}{1-\nu}\right)_s \frac{t_s^2}{6\rho t_f} \tag{4}$$

(4)=>(1)

$$\frac{t_s}{2\rho} + \left(\frac{1-\nu}{E}\right)_f \left(\frac{E}{1-\nu}\right)_s \frac{t_s^2}{6\rho t_f} = (\beta_f - \beta_s)\Delta T$$

$$\boxed{\rho = \frac{\frac{t_s}{2} + \left(\frac{1-\nu}{E}\right)_f \left(\frac{E}{1-\nu}\right)_s \frac{t_s^2}{6t_f}}{(\beta_f - \beta_s)\Delta T}} \tag{5}$$

(3) Force

$$M_f = \left(\frac{E}{1-\nu}\right)_s \frac{wt_s^{\,3}}{12\rho}$$

$$\boxed{F \approx \frac{M_s}{\ell} = \left(\frac{E}{1-\nu}\right)_s \frac{wt_s^{\,3}}{12\rho\ell}} \tag{6}$$

Force generated by thermal deflection

(4) Displacement

$$\frac{d^2z}{dx^2} = \frac{1}{\rho}$$

$$z = \frac{1}{2\rho}x^2 + c_1 x + c_2$$

at x=0, $z = 0$, $\frac{dz}{dx} = 0$

$$z = \frac{x^2}{2\rho} \quad \textbf{for} \quad x = \ell \ , \quad z = \frac{\ell^2}{2\rho} \qquad \textbf{(7)}$$

Example

	Si	**Al**
E(Pa)	**10e11**	**73e9**
β **(m/m/℃)**	**2.3e-6**	**22.5e-6**
T(μm)	**2**	**0.1**

ΔT=100℃

Neglecting poisson's ratio ν =0

w=2μm

l=10 μ m

From equation (5)

$$\rho = \frac{\frac{2\times10^{-6}}{2} + \left(\frac{10^{6}}{73\times10^{9}}\right)\frac{\left(2\times10^{-6}\right)}{6\cdot0.1\times10^{-6}}}{\left(22.5-2.3\right)10^{-6}\times100} = 0.005m$$

From equation (6)

$$F \approx \left(10^{11}\right)\frac{\left(2\times10^{-6}\right)\left(2\times10^{-6}\right)^{3}}{12\cdot0.005\cdot10\cdot10^{-6}} = 2.67\times10^{-6}N$$

From equation (7)

$$z = \frac{\ell^{2}}{2\rho} = \frac{\left(10\times10^{-6}\right)^{2}}{2\times0.005} = 10nm$$

ESS5850, F.G. Tsang
Handout 9-1, #1 p1

THERMO-MAGNETIC METAL FLEXURE ACTUATORS

H. Guckel, J. Klein, T. Christenson, K. Skrobis,
M. Laudon, E.G. Lovell

Wisconsin Center for Applied Microelectronics
Department of Electrical and Computer Engineering
University of Wisconsin
Madison, WI 53706

ABSTRACT

Deep x-ray lithography and metal plating when coupled with a sacrificial layer, SLIGA, lends itself to the fabrication of very high aspect ratio metal structures which are mechanically stiff in the substrate direction and can be very flexible in the direction parallel to the substrate. These properties can be exploited by producing a family of new flexure actuators which can produce very significant motion via thermal expansion and magnetic forces.

The magnitude of thermal effects and magnetic forces are dependent on actuator geometry. An understanding of each effect allows the design of an actuator which is dominated by one or both effects. The end result is devices intended for large motion actuators in microswitch and positioning applications. They are also useful for material constant measurements of electroplated metals.

MAGNETIC EFFECTS

The magnetic forces for the actuators of this paper are generated between two wires carrying currents in opposite directions as shown by the device in figure 1.

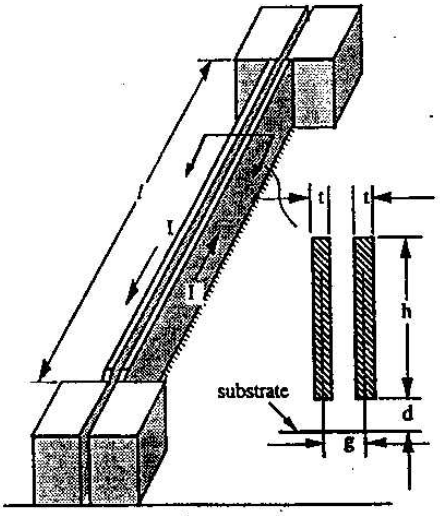

Figure 1: Magnetic effects can be seen by the beam separation when current is applied

Modeling of beams with a height of 50μm, thickness of 4μm, and a gap of 8μm show significant midlength deflection when the length is over 0.5cm. Figure 2 shows the maximum displacement of the center of the clamped-clamped beam of figure 1 as a function of length generated by a uniform magnetic pressure. The magnetic pressure is created by a 100mA current applied to each beam in opposite directions. 100mA was selected so that the resulting current density was well below the maximum current carrying capabilities of nickel. 4μm line widths were determined to be a comfortable minimum dimension to use with these rather long structures and driving currents. Figure 3 shows the maximum displacement at the center of a 0.5 cm long clamped-clamped beam as a function of beam height. Current density for this plot was the same as used in figure 2. Figure 3 shows that increasing the height of the beam beyond 40μm results in only marginal increases in beam displacement.

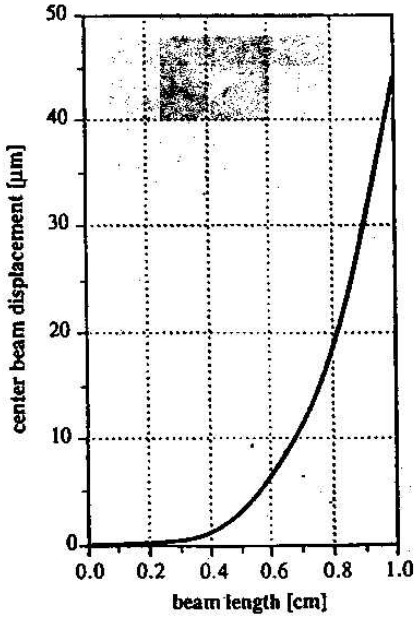

Figure 2: Magnetic beam displacement variation with beam length (h=50μm, t=4μm, g=8μm, I=100mA)

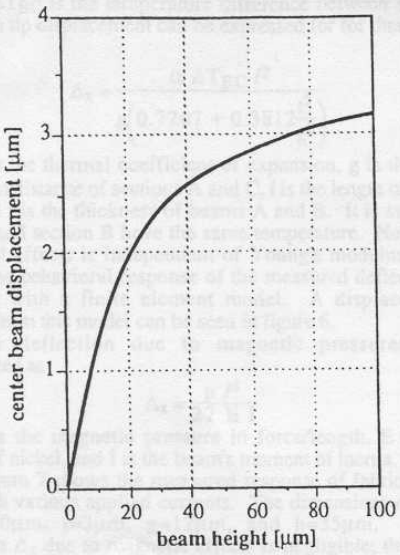

Figure 3: Magnetic beam displacement variation with beam height (l=5000μm, t=4μm, g=8μm, J=5x10^{4}A/cm^2)

THERMAL EFFECTS

Effects due to the thermal expansion of the metal structures are generated by the temperature rise of these actuators as current is applied. The temperature rise is found by balancing the I^2R power delivered to the device to the amount of energy which is dissipated through convection and radiation to the ambient and through conduction to the substrate. The heat loss by free convection and radiation is related to the structure's material, geometry, and temperature along with the temperature of the surrounding medium. Calculating heat dissipation due to convection and radiation from a beam is not trivial due to the high aspect ratio and close proximity of adjacent structures. Other variables such as fluctuations in ambient temperature, substrate temperature, and temperature dependence of physical and empirical constants make such calculations impractical. Estimates of temperature rise can be obtained through resistivity measurements of individual sections or equivalent diagnostic structures. Another way of determining the temperature rise is through the use of thermal expansion arguments and measurement of the beam defection. This later technique was used herein.

DESIGN OF A THERMAL-MAGNETIC FLEXURE

Three requirements were defined in the design of various thermal-magnetic flexures.

1) High aspect ratio beams are required to keep flexure movement in the plane of the wafer. This requirement allows for on-chip movement sensing through the use of photodiodes or contact closing.
2) Geometries of flexures should accentuate the thermal-magnetic effects to achieve large displacement or large closing forces.
3) Motion should be dominated by either thermal effects or magnetic effects to ease flexural displacement/movement predictions and to allow material constant measurements.

Asymmetry of the device provides amplification of the thermal-magnetic effects to achieve large displacement. Beam length allows simple control over which effect dominates.

THERMALLY ACTIVATED BEAM FLEXURE

The basic geometry of a thermally asymmetric driven actuator is shown in figures 4 and 5. Section C is shown to have an increased thickness relative to the rest of the device geometry resulting in a higher rigidity and a lower electrical resistance. The lower electrical resistance will provide for smaller temperature rises in this section relative to the adjacent sections when a given current is applied. This geometry difference is the asymmetrical driver for the thermally induced tip deflections. Thermal effects cause the tip of the structure to rotate clockwise as section A becomes longer than the sum of sections B and C. The magnetic pressures are small since this structure is only 0.2cm long; however, these pressures cause section A to move away from sections B and C preventing a short circuit as the tip rotates.

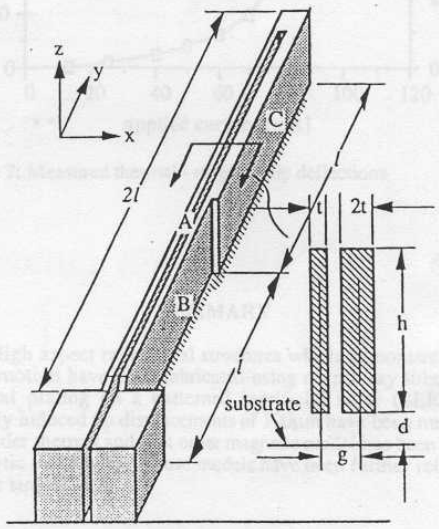

Figure 4: Basic actuator with typical dimensions l=1000μm, g=10μm, t=4μm, h=50μm

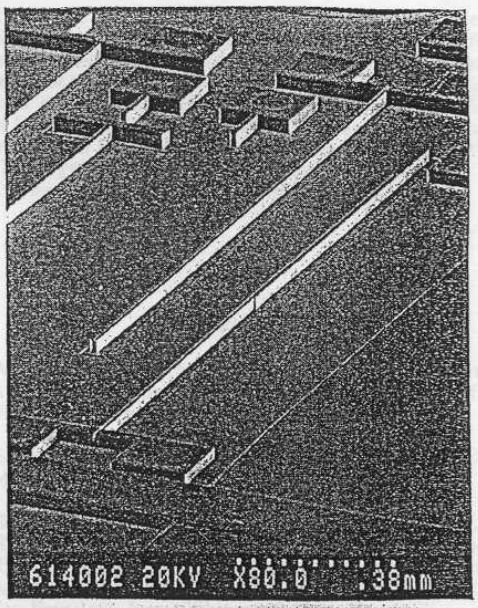

Figure 5: Fabricated actuators with different movement sensing configurations

If ΔT_{BC} is the temperature difference between segments B and C, then tip displacement can be expressed for for thermal effects as follows.

$$\Delta_x = \frac{\alpha \Delta T_{BC} l^2}{g\left(0.7707 + 0.3812\frac{t^2}{g^2}\right)} \quad (1)$$

where α is the thermal coefficient of expansion, g is the center to center beam distance of sections A and C, l is the length of sections B and C, and t is the thickness of beams A and B. It is assumed that section A and section B have the same temperature. Notice that Δ_x for thermal effects is independent of Young's modulus and beam height. The behavioral response of the measured deflections were confirmed with a finite element model. A displacement plot generated from this model can be seen in figure 6.

Tip deflection due to magnetic pressures may be approximated as

$$\Delta_x = \frac{p\, l^4}{27\, E\, I} \quad (2)$$

where p is the magnetic pressure in force/length, E is Young's modulus of nickel, and I is the beam's moment of inertia.

Figure 7 shows the measured response of fabricated nickel beams with various applied currents. The dimensions of the beam are l=1000μm, t=3μm, g=12μm, and h=35μm. For these dimensions Δ_x due to magnetic effects is negligible; therefore, the change in temperature was calculated using equation (1) and measurement of tip deflection. For these calculations a nickel resistivity of 8.5×10^{-6} ohm-cm[1], Young's modulus of (200×10^5 N/cm^2), and a temperature dependent thermal coefficient of expansion[2] was used.

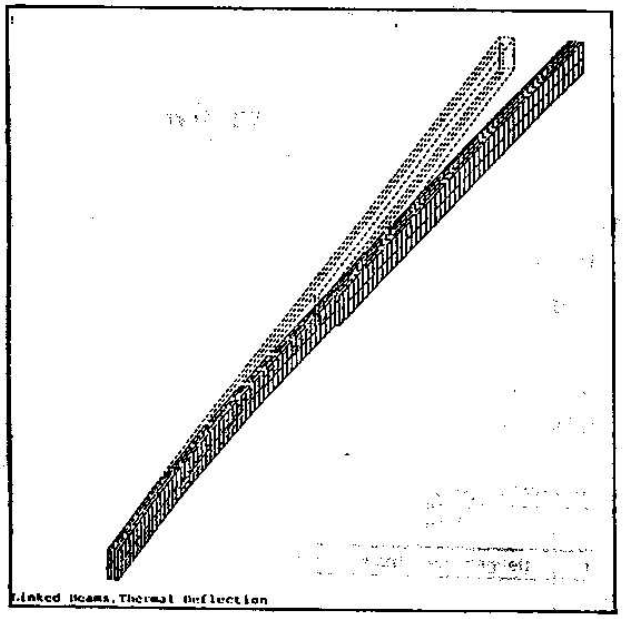

Figure 6: Finite element model of deflected thermal beam with magnetic and thermal effects included

MAGNETIC SPIRAL FLEXURE

To increase the flexure displacement due to the magnetic effect, the device must be made significantly longer. A spiral geometry allows a long beam to fit in a relatively small area. The asymmetry which amplifies displacement is due to the two beams having a different radius of curvature. These structures are currently under investigation.

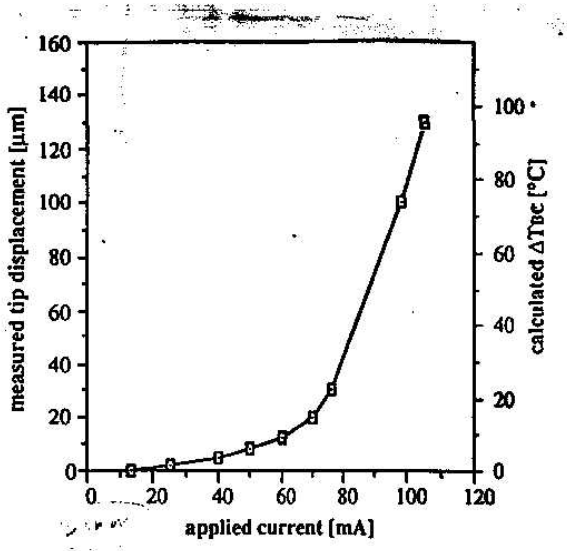

Figure 7: Measured thermal - magnetic tip deflections

SUMMARY

High aspect ratio metal structures which demonstrate large thermal motion have been fabricated using deep x-ray lithography and metal plating on a patterned sacrificial layer (SLIGA)[3]. Thermally induced tip displacements of 100μm have been measured. A first order thermal and first order magnetic model has been derived via analytic techniques. These models have been further refined by computer simulations.

ACKNOWLEDGEMENTS

This work was in part supported by the National Science Foundation under grant EET-8815285. The support of the staffs of the Center for X-ray Lithography and the Synchrotron Radiation Center for their help and the use of their facilities is acknowledged. The Center of X-ray Lithography is supported by SEMATECH Center of Excellence SCR Grant No. 88-MC-507 and the Department of Defense Naval Research Laboratory Grant No. N00014-91-J-1876. The Synchrotron Radiation Center is supported by the National Science Foundation Grant No. DMR-88-21625.

REFERENCES

[1] W. Safranek, "The Properties of Electrodeposited Metals and Alloys," 2nd Edition, American Electroplaters and Surface Finishers Society, Orlando, FL, 1986, p 256.

[2] E. Avallone, T. Baumeister, "Marks' Standard Handbook for Mechanical Engineers," 9th Ed., McGraw-Hill, 1987.

[3] H. Guckel, K.J. Skrobis, T.R. Christenson, J. Klein, S. Han, B. Choi, E.G. Lovell, "On the Application of Deep X-Ray Lithography with Sacrificial Layers to Sensor and Actuator Construction," in proceedings of Transducers '91, San Francisco, June 1991, pp. 393-396.